Stephen L. Hodson
School of Mechanical Engineering and
Birck Nanotechnology Center,
Purdue University,
West Lafayette, IN 47907
e-mail: stephen.l.hodson@gmail.com

Thiruvelu Bhuvana
Birck Nanotechnology Center,
West Lafayette, IN 47907;
Jawaharlal Nehru Centre for
Advanced Scientific Research,
Bangalore, India
e-mail: bhuv.02@gmail.com

Baratunde A. Cola
George W. Woodruff School of
Mechanical Engineering,
Georgia Institute of Technology,
Atlanta, GA 30332
e-mail: cola@gatech.edu

Xianfan Xu
School of Mechanical Engineering and
Birck Nanotechnology Center,
Purdue University,
West Lafayette, IN 47907
e-mail: xxu@purdue.edu

G. U. Kulkarni
Jawaharlal Nehru Centre for
Advanced Scientific Research,
Bangalore, India
e-mail: kulkarni@jncasr.ac.in

Timothy S. Fisher
School of Mechanical Engineering and
Birck Nanotechnology Center,
Purdue University,
West Lafayette, IN 47907
e-mail: tsfisher@purdue.edu

Palladium Thiolate Bonding of Carbon Nanotube Thermal Interfaces

Carbon nanotube (CNT) arrays can be effective thermal interface materials with high compliance and conductance over a wide temperature range. Here, we study CNT interface structures in which free CNT ends are bonded using Pd hexadecanethiolate, $Pd(SC_{16}H_{35})_2$, to an opposing substrate (one-sided interface) or opposing CNT array (two-sided interface) to enhance contact conductance while maintaining a compliant joint. The Pd weld is particularly attractive for its mechanical stability at high temperatures. A transient photoacoustic (PA) method is used to measure the thermal resistance of the palladium-bonded CNT interfaces. The interfaces were bonded at moderate pressures and then tested at 34 kPa using the PA technique. At an interface temperature of approximately 250°C, one-sided and two-sided palladium-bonded interfaces achieved thermal resistances near 10 mm^2 K/W and 5 mm^2 K/W, respectively. [DOI: 10.1115/1.4004094]

Introduction

As the size of electronic devices scales down and power densities increase, the demand for innovative cooling solutions becomes more imperative. Thermal interface materials (TIMs) such as thermal greases and gels with highly conductive particle additives are commonly used in microprocessor cooling solutions where operating temperatures are near 100°C. However, recent reliability tests on polymeric TIMs using thermogravitic analysis revealed a dramatic increase in thermal interface resistance as operating temperatures and exposure times increased [1]. Because of their high thermal conductivity, mechanical compliance, and stability over a wide temperature range, CNTs have been extensively studied as conductive elements [2–11]. Several recent reports have shown that dense, vertically aligned CNT arrays are viable alternatives to current state-of-the-art TIMs [3–11]. However, when contact sizes between a nanotube and an opposing surface become comparable to the mean free path of the dominant energy carriers, nanoscale constriction resistance becomes important. For CNT TIMs similar to those in this study, the resistive component at the CNT "free-tip" and opposing metal substrate has been shown to cause the largest constriction of heat flow in comparison to the bulk CNT and growth substrate resistances [9]. Reduction of this "free-tip" constrictive resistance using novel CNT TIM composite structures has been the subject of ongoing research.

This study aims to utilize CNT TIMs enhanced with Pd nanoparticles to achieve low thermal interface resistances suitable for electronics in a wide temperature range. In particular, two possible enhancements of Pd nanoparticle-coated CNTs on interface conductance are assessed. The first enhancement is an increase in contact area between the CNT "free-tips" and an opposing metal substrate that is formed from the Pd weld. This increase in contact area mitigates the phonon bottleneck at the CNT/metal substrate interface. Second, we consider an increase in electron density of states DOS near the Fermi level at the CNT/metal substrate interface that is a result of charge transfer between CNTs and Pd nanoparticles. In particular, we discuss the possibility of using electrons as a secondary energy carrier at the interface. One- and two-sided interfaces, comprised of CNT arrays grown on Si and Cu substrates, are bonded to opposing metal substrates using a new method that utilizes the behavior of Pd hexadecanethiolate upon

Contributed by the Electronic and Photonic Packaging Division of ASME for publication in the JOURNAL OF ELECTRONIC PACKAGING. Manuscript received December 1, 2009; final manuscript received January 13, 2011; published online June 23, 2011. Assoc. Editor: Cemal Basaran.

thermolysis. Using a transient PA technique, bulk and component thermal interface resistances of the Pd-bonded CNT interfaces were resolved.

Recent thermal resistance values for CNT based TIMs have been measured to be between 1 and 20 mm^2 K/W [3–11]. The thermal resistance values include both bonded and nonbonded interfaces, and measurements were obtained using different characterization techniques (1D reference bar, thermoreflectance, photoacoustic, and 3-omega). Weak bonding at heterogeneous interfaces, differences in phonon dispersion and density of states, and wave constriction effects are factors that could hinder further reduction in thermal contact resistance. The adverse phonon constriction can be moderated by increasing the interfacial contact area. In an effort to increase the interfacial contact area, developments in bonded and semibonded CNT TIMs have rendered thermal interface resistances as low as 1.3 mm^2 K/W [7] and 2 mm^2 K/W [10], respectively. CNTs exhibit ballistic conduction of electrons in the outermost tubes [12] and ohmic current–voltage characteristics with certain metals [13–15]. When this effect is coupled with a strong metallic-like bond at the CNT/metal substrate interface, phonon constriction could be circumvented by using electrons as a secondary energy carrier. A possible way to achieve electron transmission is through a strong CNT/metal substrate bond and sufficiently high electron DOS at the interface.

Nanoparticle-Decorated CNTs. Functionalizing CNTs with metal nanoparticles (Pt, Au, Pd, Ag, and Au) have been an area of growing interest for a diverse set of applications [16–19]. For example, a biosensor [19] involving Au/Pd nanocube-augmented SWCNTs showed significant increases in glucose sensing capabilities. The increased performance was attributed to a highly sensitive surface area, low resistance pathway at the nanocube-SWCNT interface, and selective enzyme adhesion, activity, and electron transfer at the enzyme, Au/Pd nanocube interfaces. Metal nanoparticles can adhere to CNTs through covalent or van der Waals interactions, which can lead to charge transfer. Voggu et al. [20] performed ab initio calculations on semiconducting single-walled CNTs interacting with Au and Pt nanoparticles and found a significant increase in the ratio of the metallic to semiconducting tubes when metal nanoparticles are introduced. Charge density analysis showed a decrease in electron density in the valance band of Au and an increase in the outer orbitals of C, indicating direct charge transfer. A recent study [16] also found significant changes in the Raman G-band peak intensity for pristine and silver nanoparticle-decorated metallic SWCNTs, indicating that the nanoparticles alter the electronic transitions of the tubes. With its high work function [21] and strong adhesion to CNTs, Pd has proven to be a metal that electronically couples well to CNTs [13–15,21]. Additionally, it has been suggested that efficient carrier injection from Pd monolayers to graphene can be accomplished because of the band structure that results from the hybridization between the d orbital of Pd and p-π orbital of graphene [22].

Pd Hexadecanethiolate. Metal alkanethiolates can serve as sources of metal clusters upon thermolysis and yield either metal or metal sulfide nanoparticles [23]. While metal alkanethiolates are insoluble in most organic solvents, Pd alkanethiolates have been reported to be soluble in these solvents and also exhibit repeated self-assembly [24]. The soluble nature of Pd alkanethiolates in such solvents makes them attractive for forming smooth, thin films on substrates. In this work, we used Pd hexadecanethiolate (Fig. 1) to coat the CNT sidewalls with Pd nanoparticles.

In a previous investigation by Bhuvana and Kulkarni [25], Pd hexadecanethiolate has been patterned using electron beam lithography and subsequent formation of Pd nanoparticles on thermolysis was demonstrated. Energy-dispersive spectral (EDS) values before and after thermolysis were 21:71:8 and 90:9.6:0.4 for (Pd:C:S), respectively [25]. Most notably, electrical measurements yielded resistivity values of Pd nanoparticles that were similar to that of bulk Pd.

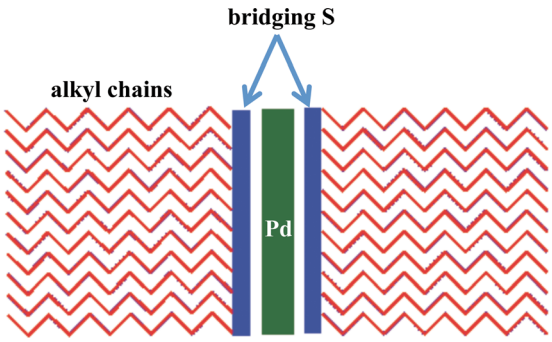

Fig. 1 $Pd(SC_{16}H_{35})_2$ structure

Experimental Details

CNT Growth by Microwave-Plasma CVD. In manner similar to that described by Xu and Fisher [5], an electron beam evaporative system was used to deposit a trilayer metal catalyst stack consisting of 30 nm Ti, 10 nm Al, and 3 nm Fe on polished intrinsic Si substrates. For a two-sided interface, the tri-layer catalyst was deposited on both a Si substrate and 25 μm thick Cu foil purchased from Alfa Aesar (Puratronic®, 99.999% metals basis). Vertically oriented CNT arrays of moderately high density were then synthesized in a SEKI AX5200S microwave plasma chemical vapor deposition (MPCVD) system described in detail in previous work [26]. In summary, the growth chamber was evacuated to 1 Torr and purged with N_2 for 5 min. The samples were heated in N_2 (30 sccm) to a growth temperature of 900°C. The N_2 valve was then closed and 50 sccm of H_2 was introduced to maintain a pressure of 10 Torr in the growth chamber. After the chamber pressure stabilized, a 200 W plasma was ignited and 10 sccm of CH_4 was introduced to commence 10 min of CNT synthesis. The samples were imaged using a Hitachi field-emission scanning electron microscope (FESEM). Figure 2 contains images of the vertically oriented CNT arrays synthesized on Si. CNT arrays grown on Cu foil are similar. The array densities were estimated to be approximately 10^8–10^9 CNTs/mm^2. This estimation was conducted by manually counting CNTs from five different array locations at a moderate magnification in the FESEM. The average CNT diameter for each array was approximately 30 nm while the array heights were approximately, 15–25 μm.

Preparation of Pd TIMs. For preparation of Pd hexadecanethiolate, an equimolar solution of $Pd(OAc)_2$ (Sigma Aldrich) in toluene was added to hexadecanethiol and stirred vigorously. Following the reaction, the solution became viscous and the initial yellow color deepened to an orange-yellow color. The hexadecanethiolate was washed with methanol and acetonitrile to remove excess thiol and finally dissolved in toluene to obtain a 200 mM solution. Using a micropipette, approximately 16 μL of Pd hexadecanethiolate was added to the CNT array. The CNT array was then heated for 5 min at 130°C to evaporate the toluene. Finally, the components of the two TIM structures tested were formed by sandwiching the substrates under a pressure of 273 kPa and commencing thermolysis by baking at 250°C for 2 h in air. The Si/CNT/Ag foil structure consisted of Si/CNT and Ag while the Si/CNT/CNT/Cu structure comprised of Si/CNT and CNT/Cu. Figure 3 contains an FESEM image of the CNT array after thermolysis at 250°C. The Pd nanoparticles that decorate the CNT walls range from approximately 1 to 10 nm. Similar to other studies [16,27], we assume that Pd nanoparticles preferentially attach to defect sites in the CNT sidewalls. The control samples (no Pd

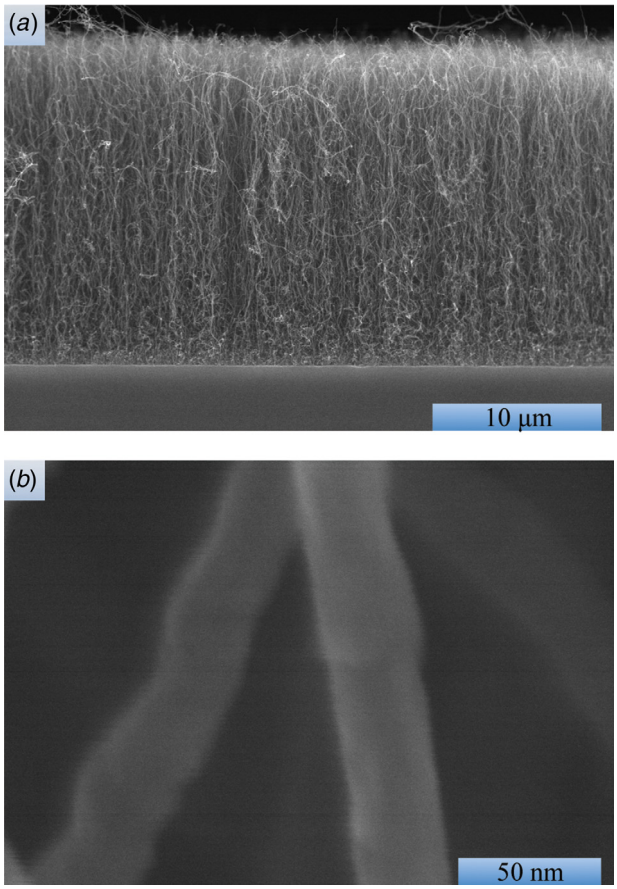

Fig. 2 CNT arrays synthesized on Si substrate. (*a*) FESEM cross-section image illustrating array height and (*b*) FESEM image illustrating CNT diameter.

hexadecanethiolate and only toluene) were prepared under the same heating and loading conditions as above.

Photoacoustic Thermal Measurements. A transient photoacoustic (PA) technique that has been described in detail previously [8,11] was used to characterize thermal interface resistances. Figure 4 contains cross-sectional sketches for each multilayer sample type tested, and Fig. 5 shows the experimental setup. For a multilayer structure, the PA technique can resolve both bulk and component resistances in which the bulk resistance R_{bulk} in Fig. 4(*a*) is defined as

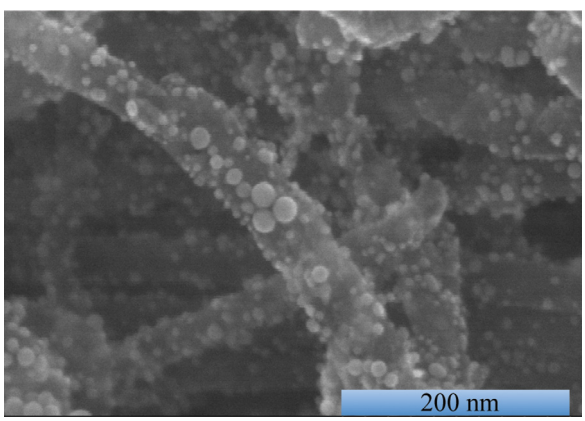

Fig. 3 Post-thermolysis FESEM image of CNT array on Si substrate

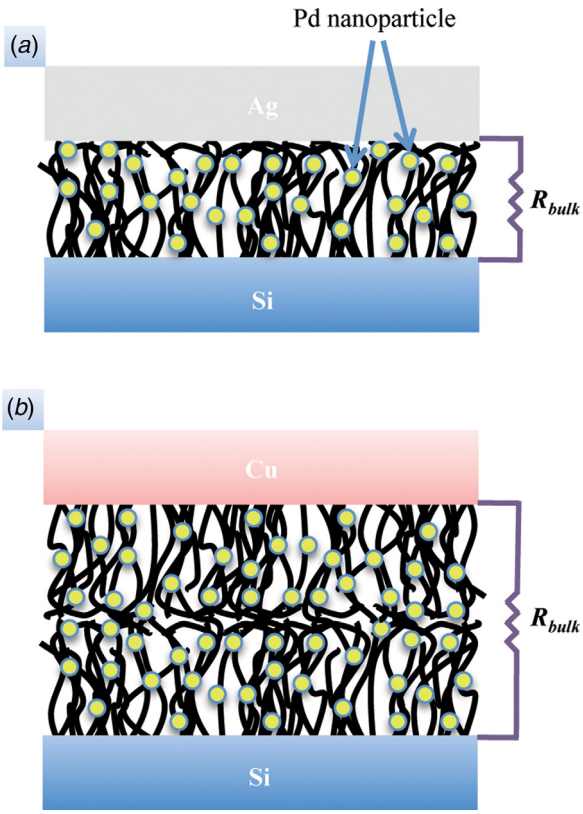

Fig. 4 Cross-sections of various TIM structures tested. (*a*) Si/CNT/Ag and (*b*) Si/CNT/CNT/Cu.

$$R_{bulk} = R_{Si-CNT} + R_{CNT} + R_{CNT-Ag} \quad (1)$$

where R_{CNT} is the resistance of the CNT array and $R_{Si\text{-}CNT}$ and $R_{CNT\text{-}Ag}$ are the contact resistances at the Si-CNT and CNT-Ag interfaces, respectively [28]. Briefly, in a given PA measurement, the sample surface is surrounded by a sealed acoustic cell that is pressurized with He gas at 34 kPa. The sample is then heated over a range of frequencies by a 350 mW, modulated laser source. The thermal response of the multilayer sample induces a transient temperature field in the gas that is related to cell pressure. A microphone housed in the chamber wall measures the phase shift of the temperature-induced pressure response in the acoustic chamber. Using the acoustic signal in conjunction with the model developed in Ref. [8], which is based on a set of one-dimensional heat conduction equations, thermal interface resistances are determined using a least-squares fitting method.

Results and Discussion

The PA technique was used to resolve bulk thermal interface resistances of one- and two-sided TIMs with configurations of Si/CNT/Ag and Si/CNT/CNT/Cu. The latter samples had CNT

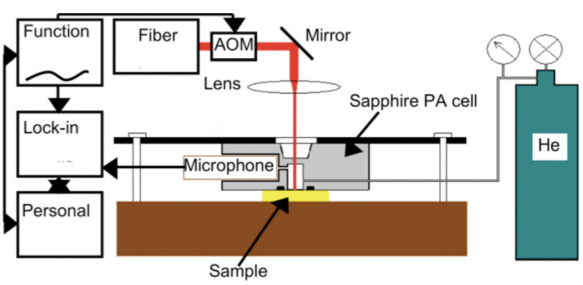

Fig. 5 Photoacoustic experimental setup

arrays grown on both the Si and Cu substrates, and the resulting interface formed a two-sided, Velcro^{TM}-like structure (see Fig. 4(*b*)). In addition, component resistances were resolved on a separate Si/CNT/Ag sample to elucidate possible mechanisms for enhanced performance. We note that the sample used for measuring component resistances was not identical to those used to measure overall resistance. Specifically, a lower Pd thiolate concentration and bonding pressure were employed in order to intentionally yield a sample with poor thermal resistance such that the effects of the Pd bonding could be better distinguished.

In order to ensure proper operation of the pressure-field microphone used in the PA setup, the maximum temperature tested was 250°C, and the chamber pressure was limited to 34 kPa. Bulk resistance measurements for the Si/CNT/Ag and Si/CNT/CNT/Cu samples were taken in a temperature range of 27°C to 250°C while the component resistance measurement on the second Si/CNT/Ag sample was performed at 27°C. Figure 6 shows bulk thermal resistance values as a function of temperature for the Si/CNT/Ag and Si/CNT/CNT/Cu samples. The resolved component resistances for the second Si/CNT/Ag are tabulated in Table 1.

Within the temperature range, the Si/CNT/Ag and Si/CNT/CNT/Cu structures decorated with Pd nanoparticles significantly outperform the structures without Pd nanoparticles where the average thermal resistance value for the Pd nanoparticle-enhanced structures was 11 mm^2 K/W and 5 mm^2 K/W, respectively. Averaging thermal resistances across the temperature range yielded reductions of thermal resistance across the interface of approximately 50% in both cases. In addition, all structures exhibited only small variations in performance across the temperature range, indicating thermal stability and applicability to high-temperature devices. Due to the fact that Pd contains toluene, the effect of toluene on the morphology of the CNT array and ultimately the thermal performance needs to be addressed. Therefore, an additional set of samples were fabricated in which only toluene was added to the array. These samples were also subject to the same heating and loading conditions and subsequently tested by PA. The interface resistances tabulated in Table 2 indicate that while toluene is expected to significantly alter the CNT array morphology, its effect on thermal transport is negligible compared to the welding process that occurs during thermolysis. We note that the toluene treated sample tested at a comparable resistance to the Si/CNT/Ag sample but remained within the instrument error. Similar to Ref. [8], the error estimates in Fig. 6 and Tables 1 and 2 are based on the instrument error that dominates over uncertainties based on the confidence interval from the regression analysis.

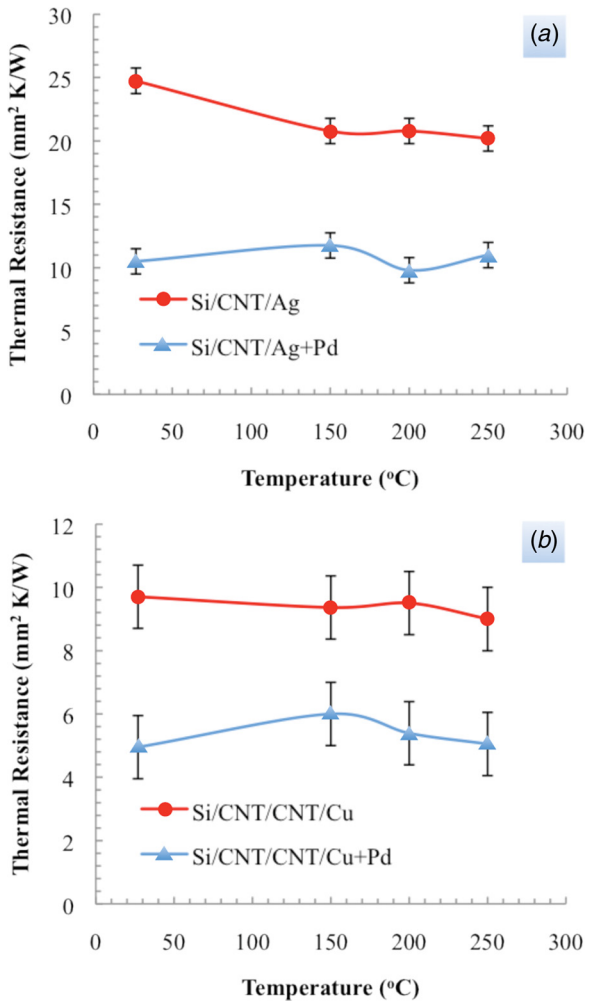

Fig. 6 Bulk thermal interface resistance as a function of temperature. (*a*) Si/CNT/Ag w/ and w/o Pd nanoparticles and (*b*) Si/CNT/CNT/Cu w/ and w/o Pd nanoparticles.

Table 1 Component thermal resistances for Si/CNT/Ag structure at 27°C with and without Pd nanoparticles

Sample	$R_{Si\text{-}CNT}$ (mm^2 K/W)	R_{CNT} (mm^2 K/W)	$R_{CNT\text{-}Ag}$ (mm^2 K/W)
Si/CNT/Ag	2 ± 1	<1	40 ± 4
Si/CNT/Ag + Pd	<1	<1	15 ± 1

Thermal testing was proceeded by assessment of the Pd enhanced bond by FESEM. Figures 7 and 8 contain images of the structures after the bond was broken and the substrates were separated. For the Si/CNT/Ag structure, the Si and Ag foil substrates are depicted in Fig. 7 while the Si and Cu foil substrates of the Si/CNT/CNT/Cu structure corresponds to Fig. 8. Clumps of CNTs that either remain attached to their Si growth substrate or are bonded to the Ag foil are readily seen in Fig. 7. Additionally, Fig. 7(*a*) shows a mesoscopic chasm in the CNT array and at higher magnification, and Fig 7(*b*) reveals sites in which CNTs were once attached to the growth substrate. Examination of Figs. 7(*c*) and 7(*d*) indicate the clumps of CNTs are also attached to the Ag foil. From a thermal perspective, these CNT clumps most likely serve as hubs for heat transport between the array and the Ag foil. We note that an additional quantitative assessment comparing the bond strength at the growth and Ag foil substrates would complement these observations and plan to do so in future work. In lieu of this assessment, we postulate that upon detachment, fracture of the bond occurs at the interfaces as well as within the CNT array. Figure 8 shows similar features throughout the landscapes of both the Si and Cu foil substrates. While not observable in the Si/CNT/Ag structure, the CNT arrays in Figs. 8(*a*) and 8(*c*), in particular the latter, resemble a topographical landscape indicating that significant bonding occurred at or around the CNT/CNT interface and most likely depends on the extent that one array penetrates into the other.

The results in Table 1 indicate that reductions in bulk thermal resistance between decorated and undecorated TIMs occurred at the Si–CNT and CNT–Ag interfaces, with the latter having the largest reduction. These results are congruent with Ref. [9] in which the dominant thermal resistance was at the CNT "free-tip" interface as opposed to the growth substrate interface where the

Table 2 Bulk thermal resistances for Si/CNT/Ag structures at 27°C with and without Pd nanoparticles and/or toluene

Sample	$R_{Si\text{-}CNT}$ (mm^2 K/W)
Si/CNT/Ag	21 ± 1
Si/CNT/Ag + toluene	21 ± 1
Si/CNT/Ag + Pd	14 ± 1

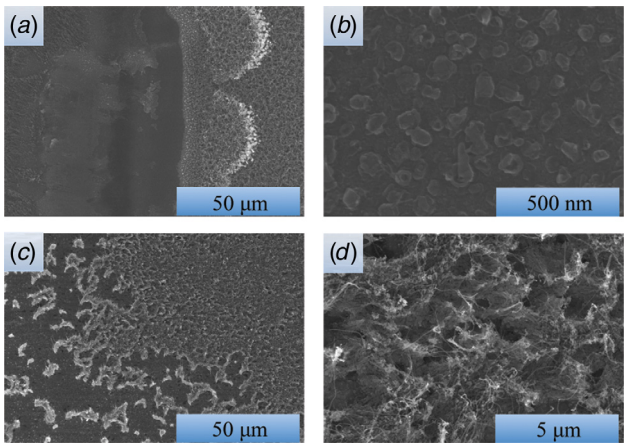

Fig. 7 SEM images of Si/CNT/Ag foil structure after detachment. (*a*) and (*b*) correspond to the Si substrate while (*c*) and (*d*) correspond to the Ag foil.

CNTs are well adhered. This significant reduction at the CNT–Ag interface can be attributed to two mechanisms, both comprising of nano- and mesoscopically sized contact regions as seen in Figs. 7 and 8. First, upon thermolysis, a strong bond between at the CNT/Ag was created such that greater contact area was achieved and we attribute the majority of improvement to the reduced phonon reflection at the CNT/Ag interface. In a previous study [9], the authors concluded that the increase in contact area reduced phonon reflection at the boundary consisting of nanosized contacts and provided enhanced pathways for heat conduction. Similarly, we postulate that the primary effect of Pd nanoparticles is to enlarge individual contact points both at the CNT/CNT and CNT/substrate interfaces. In a broader perspective relative to length scales, the ballistic component of constriction resistance that dominates its diffusive counterpart [28] would be more influential in an unbonded structure that primarily consists of many nanosized contact points as opposed to a Pd bonded structure in which the aggregated effect of Pd nanoparticles gives rise to more mesoscopically sized contact regions.

Second, in previous work by Bhuvana and Kulkarni [25], thermal treatment of Pd hexadecanethiolate at 230°C in air produced metallic Pd nanowires with a specific electrical resistivity near 0.300 $\mu\Omega$ m. Similarly, thermal treatment of structures in this study could have produced a metallic-like bond between CNT free ends and Ag foil via Pd nanoparticles in which a higher electron DOS near the Fermi level at the CNT/Ag interface was established. We also note that two types of contacts can exist at a CNT/metal interface: side- and end-contacted. Although the general orientation of the dense, CNT arrays in Fig. 2(*a*) are vertical, we assume that the majority of the contacts have side-contacted geometries upon compression into an interface. For nonbonded, side-contacted geometries, the contact quality depends on tunneling of electrons across an energy barrier created by van der Waals interaction at the metal/CNT interface [29] and since the physical separation between the metal and CNT is comparable to the carbon/metal bond length, tunneling depends on the chemical composition and configuration of electronic states at the surface [13]. If we consider Ag making uniform contact to graphene and the transmission of an electron across the CNT/Ag interface, then in-plane wave vector conservation is enforced and for good coupling, the metal Fermi wave vector ($k_{f,Ag} = 1.2$ Å^{-1}) should be comparable to that of graphene ($k_{f,graph.} = 4\pi/3a_o = 1.70$ Å^{-1}) [29,30]. Under weak coupling assumption (i.e., van der Waals interaction), calculated transmission probabilities at a uniform metal/graphene contact have been shown to exhibit a monotonic increase with contact length depending on CNT chirality [30]. Indeed, the transmission probabilities reported in Ref. [30] are quite small and therefore serve as a lower limit because the calculations were based on coupling strengths $\sim O(10^{-3})$ eV. Furthermore, if the coupling strength were increased via a metallic-like bond, then higher transmission probabilities could be achieved.

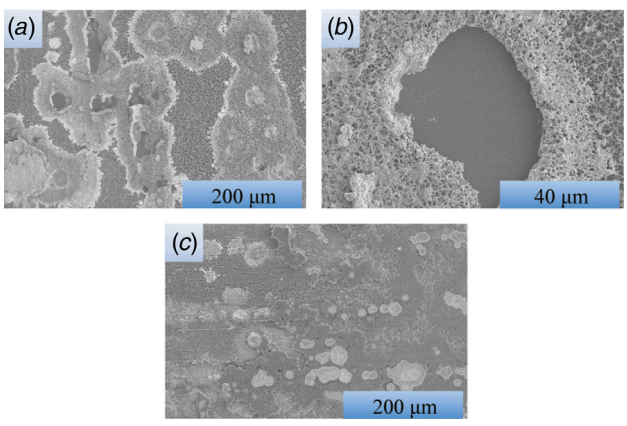

Fig. 8 SEM images of Si/CNT/CNT/Cu structure after detachment. (*a*) and (*b*) correspond to the Si substrate while (*c*) corresponds to the Cu foil.

For larger diameter tubes, such as the CNTs in the present work, wavevector conservation becomes increasingly important [30]. However, such conservation principles can be relaxed when disorder (defects and impurities) are present [30]. Plasma-enhanced chemical vapor deposition (PECVD) grown CNTs in previous work have exhibited relatively high defects at the sidewalls due to plasma etching [26,31,32]. Thus, the additional disorder from sidewall defects caused by PECVD synthesis and Pd impurities at the CNT/Ag interface could relax wavevector conservation constraints. In this case, additional scattering from defects and Pd impurities could increase the transmission probability across the CNT/Ag interface, mediated by the presence of the Pd nanoparticles. However, for CNT/metal contacts as opposed to graphene/metal, it has been shown that coupling of electronic states between the CNT and metal will exist regardless of scattering from defects and impurities [33]. We expect similar effects to be operative for the two-sided TIM configuration (Fig. 4(*b*)), with most of the improvement localized at the CNT/CNT interface.

Conclusions

In this study, CNT TIMs enhanced with Pd nanoparticles were fabricated using a previously developed method for CNT synthesis and a new process for bonding interfaces using Pd hexadecanethiolate. A transient photoacoustic technique was used to resolve bulk and component thermal interface resistances. All structures enhanced with Pd nanoparticles exhibited markedly improved thermal performance and thermal interface resistances that are comparable to previously reported values in the literature and that outperform most state-of-the-art TIMs used in industry. We attribute the majority of improved performance to the strong Pd weld that reduced phonon reflection at the interface by increasing the contact area between the CNT "free-tips" and an opposing metal substrate. In addition, we considered utilizing electrons as a secondary energy carrier at the interface because of an increase in electron density of states at the CNT/Ag interface and offered discussion on the dependence that electron transmission has on wave vector conservation and disorder. With thermal stability across a wide temperature range, these structures are suitable for a variety of applications, particularly high-temperature electronics. Further investigation of energy and charge transport mechanisms at interfaces and Raman characterization of the CNT TIMs will elucidate the results of this study. Lastly, additional optimization related to coating and thermolysis of the Pd hexadecanethiolate solution on the CNT arrays could further reduce thermal interface resistance.

Acknowledgment

T. Bhuvana and G. U. Kulkarni gratefully acknowledge the support from the Department of Science and Technology, Government of India. S. Hodson and T.S. Fisher gratefully acknowledge partial support of this work from Raytheon as part of the DARPA Nano Thermal Interfaces Program.

References

[1] Prasher, R., 2006, "Thermal Interface Materials: Historical Perspective, Status, and Future Directions," Proc. IEEE, **94**(8), pp. 1571–1586.
[2] Biercuk, M. J., Llanguno, M. C., Radosavlievic, Hyun, J. K., Johnson, A. T., and Fischer, J. E., 2002, "Carbon Nanotube Composites for Thermal Management," Appl. Phys. Lett., **80**(15), pp. 2767–2769.
[3] Panzer, M. A., Zhang, G., Mann, D., Hu, X., Pop, E., Dai, H., and Goodson, K. E., 2008, "Thermal Properties of Metal-Coated Vertically Aligned Single-Wall Nanotube Arrays," ASME J. Heat Transfer, **130**, p. 052401.
[4] Xu, J., and Fisher, T. S., 2006, "Enhanced Thermal Contact Conductance using Carbon Nanotube Array Interfaces," IEEE Trans. Compon. Packag. Technol., **29**(2), pp. 261–267.
[5] Xu, J., and Fisher, T. S., 2006, "Enhancement of Thermal Interface Materials With Carbon Nanotube Arrays," Int. J. Heat Mass Transfer, **49**, pp. 1658–1666.
[6] Tong, T., Zhao, Y., Delzeit, L., Kashani, A., Meyyappan, M., and Majumdar, A., 2007, "Dense Vertically Aligned Multiwalled Carbon Nanotube Arrays as Thermal Interface Materials," IEEE Trans. Compon. Packag. Technol., **30**(1), pp. 92–100.
[7] Hu, X., Pan, L. S., Gu, G., and Goodson, K. E., 2009, "Superior Thermal Interfaces Made by Metallically Anchored Carbon Nanotube Arrays," *Proceedings of ASME Summer Heat Transfer Conference*, San Francisco, CA.
[8] Cola, B. A., Hu, J., Cheng, C., Hu, H., Xu, X., and Fisher, T. S., 2007, "Photoacoustic Characterization of Carbon Nanotube Array Interfaces," J. Appl. Phys., **101**(5), p. 054313.
[9] Cola, B. A., Xu, X., and Fisher, T. S., 2007, "Increased Real Contact in Thermal Interfaces: A Carbon Nanotube/Foil Material," Appl. Phys. Lett., **90**(9), p. 093513.
[10] Cola, B. A., Hodson, S. L., Xu, X., and Fisher, T. S., 2008, "Carbon Nanotube Array Thermal Interfaces Enhanced with Paraffin Wax," *Proceedings of ASME Summer Heat Transfer Conference*, Jacksonville, FL.
[11] Cola, B. A., Capano, M. A., Amama, P. B., Xu, X., and Fisher, T. S., 2008, "Carbon Nanotube Array Thermal Interfaces for High-Temperature Silicon Carbide Devices," Nanoscale Microscale Thermophys. Eng., **12**(3), pp. 228–237.
[12] Frank, S., Poncharal, P., Wang, Z. L., and de Heer, W. A., 1998, "Carbon Nanotube Quantum Resistors," Science, **280**(5370), pp. 1744–1746.
[13] Ngo, Q., Petranovic, D., Krishnan, S., Cassell, A. M., Ye, Q., Li, J., Meyyappan, M., and Yang, C. Y., 2004, "Electron Transport Through Metal-Multiwall Carbon Nanotube Interfaces," IEEE Trans. Nanotechnol., **3**(2), pp. 311–317.
[14] Mann, D., Javey, A., Kong, J., Wang, Q., and Dai, H., 2003, "Ballistic Transport in Metallic Nanotubes With Reliable Pd Ohmic Contacts," Nano Lett., **3**(11), pp. 1541–1544.
[15] Matsuda, Y., Deng, W., and Goddard, W. A., 2007, "Contact Resistance Properties Between Nanotubes and Various Metals from Quantum Mechanics," J. Phys. Chem. C, **111**(29), pp. 11113–11116.
[16] Lin, Y., Watson, K. A., Fallbach, M. J., Ghose, S., Smith, J. G., Jr., Delozier, D., Cao, W., Crooks, R. E., and Connell, J. W., 2009, "Rapid, Solventless, Bulk Preparation of Metal Nanoparticle-Decorated Carbon Nanotubes," ACS Nano, **3**(4), pp. 871–884.
[17] Wildgoose, G. G., Banks, C. E., and Compton, R. G., 2006, "Metal Nanoparticles and Related Materials Supported on Carbon Nanotubes: Methods and Applications," Small, **2**(2), pp. 182–193.
[18] Georgakilas, V., Gournis, D., Tzitzios, V., Pasquato, L., Guldi, D. M., and Prato, M., 2007, "Decorating Carbon Nanotubes With Metal or Semiconductor Particles," J. Mater. Chem., **17**(26), pp. 2679–2694.
[19] Claussen, J. C., Franklin, A. D., Haque, A., Porterfield, D. M., and Fisher, T. S., 2009, "Electrochemical Biosensor of Nanocube-Augmented Carbon Nanotube Networks," ACS Nano, **3**(1), pp. 37–44.
[20] Voggu, R., Pal, S., Pati, S. K., and Rao, C. N. R., 2008, "Semiconductor to Metal Transition in SWNTs Caused by Interaction With Gold and Platinum Nanoparticles," J. Phys.-Condens. Matter, **20**(21), p. 215211.
[21] Javey, A., Guo, J., Wang, Q., Lundstrom, M., and Dai, H., 2003, "Ballistic Carbon Nanotube Field-Effect Transistors," Nature, **424**(6949), pp. 654–657.
[22] Nemec, N., Tomanek, D., and Cuniberti, G., 2006, "Contact Dependence of Carrier Injection in Carbon Nanotubes: An *Ab Initio* Study," Phys. Rev. Lett., **96**(7), p. 076802.
[23] Carotenuto, G., and Martorana, B., 2003, "A Universal Method for the Synthesis of Metal and Metal Sulfide Clusters Embedded in Polymer Matrices," J. Mater. Chem., **13**(12), pp. 2927–2930.
[24] Thomas, P. J., Lavanya, A., Sabareesh, V., and Kulkarni, G. U., 2001, "Self-Assembling Bi-Layers of Palladium Thiolates in Organic Media," Proc. Indian Acad. Sci.-Chem. Sci., **113**(5–6), pp. 611–619.
[25] Bhuvana, T., and Kulkarni, G. U., 2008, "Highly Conducting Patterned Pd Nanowires by Direct-Write Electron Beam Lithography," ACS Nano, **2**(3), pp. 457–462.
[26] Maschmann, M. R., Amama, P. B., Goyal, A., Iqbal, Z., Gat, R., and Fisher, T. S., 2006, "Parametric Study of Synthesis Conditions in Plasma-Enhanced CVD of High-Quality Single-Walled Carbon Nanotubes," Carbon, **44**(1), pp. 10–18.
[27] Zoval, J. V., Biernacki, P. R., and Penner, R. M., 1996, "Implementation of Electrochemically Synthesized Silver Nanocrystallites for Preferential SERS Enhancement of Defect Modes on Thermally Etched Graphite Surfaces," Anal. Chem., **68**(9), pp. 1585–1592.
[28] Cola, B. A., Xu, J., and Fisher, T. S., 2009, "Contact Mechanics and Thermal Conductance of Carbon Nanotube Array Interfaces," Int. J. Heat Mass Transfer, **52**(15–16), pp. 3490–3503.
[29] Tersoff, J., 1999, "Contact Resistance of Carbon Nanotubes," Appl. Phys. Lett., **74**(15), pp. 2122–2124.
[30] Anantram, M. P., Datta, S., and Xue, Y., 2000, "Coupling of Carbon Nanotubes to Metallic Contacts," Phys. Rev. B, **61**(20), p. 14219–14224.
[31] Matthews, K., Cruden, B. A., Chen, B., Meyyappan, M., and Delzeit, L., 2002, "Plasma-Enhanced Chemical Vapor Deposition of Multiwalled Carbon Nanofibres," J. Nanosci. Nanotechnol., **2**(5), pp. 475–480.
[32] Amama, P. B., Cola, B. A., Sands, T. D., Xu, X., and Fisher, T. S., 2007, "Dendrimer-Assisted Controlled Growth of Carbon Nanotubes for Enhanced Thermal Interface Conductance," Nanotechnology, **18**(38), p. 385303.
[33] Delaney, P., and Ventra, M. D., 1999, "Comment on 'Contact Resistance of Carbon Nanotubes," Appl. Phys. Lett., **75**(25), pp. 4028–4029.